

Smooth Teeth: Why Multipoles Are Perfect Gears

Johannes Schönke

Okinawa Institute of Science and Technology Graduate University, Onna, Okinawa 904 0495, Japan
(Received 18 September 2015; revised manuscript received 29 October 2015; published 22 December 2015)

A type of gear is proposed based on the interaction of individual multipoles. The underlying principle relies on previously unknown continuous degenerate ground states for pairs of interacting multipoles which are free to rotate around specific axes. These special rotation axes, in turn, form a one-parameter family of possible configurations. This allows for the construction of magnetic bevel gears with any desired inclination angle between the in- and output axes. Further, the design of gear systems with more than two multipoles is possible and facilitates tailored applications. Ultimately, an analogy between multipoles and mechanical gears is revealed. In contrast to the mechanical case, the multipole “teeth” mesh smoothly. As an illustrative application, the example of a quadrupole-dipole interaction is then used to construct a 1:2 gear ratio.

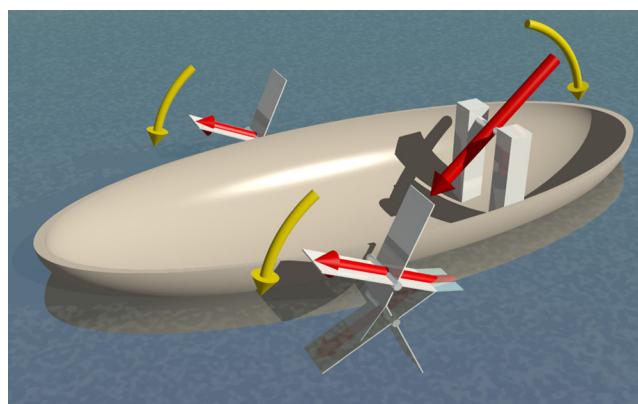
DOI: [10.1103/PhysRevApplied.4.064007](https://doi.org/10.1103/PhysRevApplied.4.064007)

I. INTRODUCTION

A very useful device in a chemistry lab is the magnetic stirrer, but magnetic couplings like this one are found not only in scientific equipment—even the newest milk frothers use them to create the perfect topping for your coffee. On a smaller scale, magnetic mechanisms and couplings are used in microfluidic systems to serve as pumps, valves, or mixers [1,2], and on the even smaller scales of the nano-world, molecular machines are, in fact, restricted to electronic or magnetic interactions [3]. What if we could use such elementary structures like dipoles or quadrupoles individually to transmit rotary motion in a very flexible way? Today’s industrial magnetic gear designs are based on arrays of many permanent magnets which mimic the teeth of classical mechanical gears (for a review, see Ref. [4] and the next paragraph). Here we propose gears fundamentally different from these designs, based on the interaction of individually rotating multipoles. This approach allows us to construct gears with inclined axes and leads further to configurations like the one depicted in Video 1, which consists of three dipoles that form a smooth coupling. Finally, we uncover an analogy between multipoles and mechanical gears and demonstrate that a quadrupole and a dipole can be used to construct a gear ratio of 1:2 (see Video 3). The findings in this paper initiate questions for theoretical physics about the necessary conditions for which smooth couplings between multipoles are possible. At the same time, the constructions reported here can already be used in many different applications, a few of them we mention above.

Although the mechanical gear was invented in antiquity, the idea of a magnetic gear is only a hundred years old [5]. Magnetic gears have many advantages: being free of contact, they are not subject to mechanical wear, need no lubrication, possess inherent overload protection, are

noiseless, are highly reliable, and operate with reduced maintenance. Moreover, the input and output can be physically isolated. With the appearance of strong magnets based on alloys of rare-earth elements, the interest in magnetic gears grew because of increased torque transmission capabilities [6]. In the last decade, innovative designs for the magnetic gear topology further increased the possible torque densities. Today, magnetic gears can compete with mechanical realizations in industrially relevant applications. Most of the designs are coaxial [7–16] and include intricate constructions like planetary [17] and cycloid gears [18]. Biaxial systems can also be found [19,20]. Specifically related to the current work is the discussion of the undesirable cogging torque [13,14,16,17], namely, periodic variation of the transmitted torque during



VIDEO 1. (Animated version online.) Three interacting dipoles (red arrows) form a smooth coupling capable of driving a paddle boat. If the central dipole is rotated, the other two dipoles at the paddles rotate accordingly (the motion is symbolized by yellow arrows in the nonanimated version). Up to an overall scaling in size, the positioning of the dipoles is crucial. Only in this specific triangle geometry does the smooth coupling work (Fig. 5).

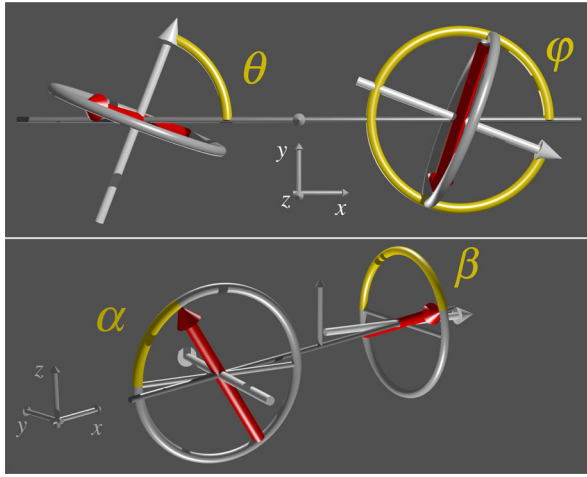


FIG. 1. Definition of the angles which describe the rotation of the dipoles (red). The upper panel introduces the two angles θ and φ which set the positions of the rotation axes (light gray). The rotation axes are restricted to lie in the x - y plane. The angles θ and φ (and, therefore, the rotations axes) are fixed for a given configuration. The lower panel introduces the angles α and β which correspond to the 2 degrees of freedom the system possesses. α and β describe the actual orientation of the two dipoles during rotation.

revolution induced by the geometry and magnetization pattern of the gear. So far, the only realization capable of avoiding cogging torque is the coaxial gear with a 1:1 ratio, generally referred to as the “synchronous axial coupling,” first thoroughly analyzed in Refs. [21,22].

II. TWO INTERACTING DIPOLES

We begin with the following problem statement: place a set of multipoles in space and allow them to rotate around predefined axes. Under which conditions (regarding positioning and orientation of the axes) do these multipoles possess a continuous ground state (CGS) in the sense that the lowest possible energy configuration is degenerate? Once such a state is found, we can rotate one of the multipoles, and the others will follow without any counterforce; a smooth coupling is created without any cogging torque.

If the system consists of dipoles only, the interaction energy reads for a total number of N dipoles

$$E_N = \sum_{i < j}^N \frac{\mathbf{m}_i \cdot \mathbf{m}_j |\mathbf{r}_{ij}|^2 - 3(\mathbf{m}_i \cdot \mathbf{r}_{ij})(\mathbf{m}_j \cdot \mathbf{r}_{ij})}{|\mathbf{r}_{ij}|^5}, \quad (1)$$

where $\mathbf{m}_1, \dots, \mathbf{m}_N$ are the variable dipole moments, and \mathbf{r}_{ij} denotes the fixed relative position vector between dipole i and j .

First, we consider the case of two dipoles separated by a fixed distance d that are allowed to rotate only around fixed axes orthogonal to their dipole moment; see Fig. 1. In this

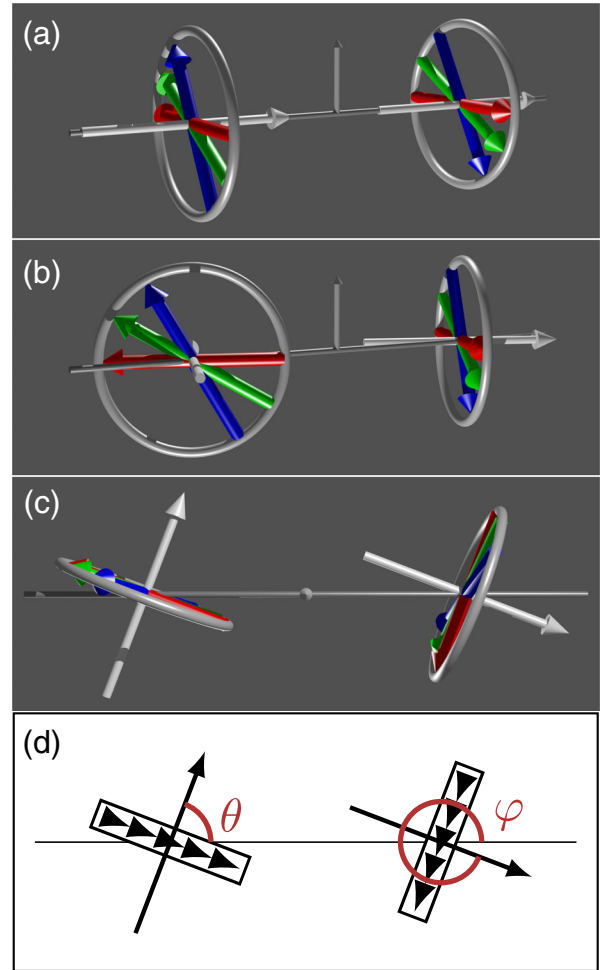


FIG. 2. (a) The trivial example for a continuous ground state created by two dipoles which are allowed to rotate about a common axis. The (red, green, blue) colored arrows illustrate the dipole motion in the ground state for three different times. The light gray arrows define the prescribed rotation axes, and the rings guide the eye regarding the path the colored arrows take while rotating. The small upward arrow in the middle is normal to the horizontal plane. (b) Example of a continuous ground state created by two dipoles which are allowed to rotate about two orthogonal axes. (c) The same configuration as in (b) but viewed from the top along the normal vector of the horizontal plane in which the rotation axes are lying. (d) Schematic of the view from the top defining the positions of the rotation axes via the angles θ and φ .

case, there is an obvious trivial solution to the posed problem: the two rotation axes are aligned, and the two dipoles are antiparallel [Fig. 2(a)]. This configuration is precisely the previously mentioned synchronous axial coupling realized with two dipoles. The principle behind this solution is not related to the nontrivial findings described below because it does not rely on dipole interactions. This system describes a continuous state simply because it exhibits an obvious rotational symmetry about the one and only rotation axis.

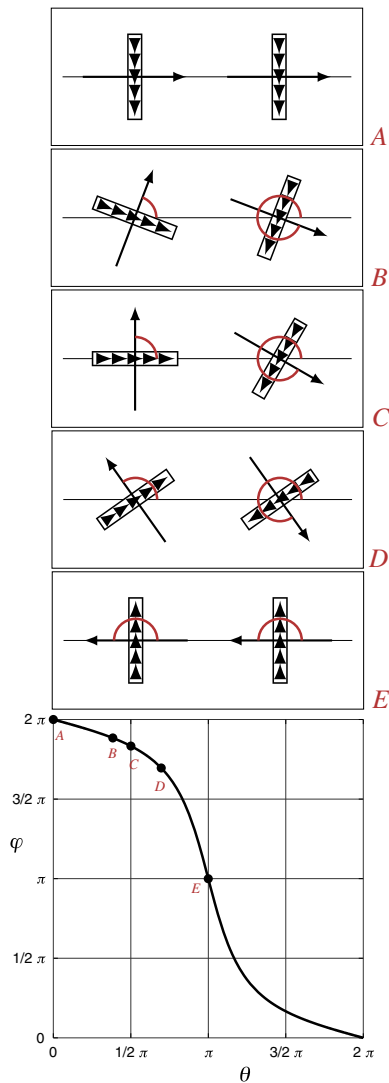


FIG. 3. Configurations of continuous ground states created by two dipoles which are allowed to rotate about fixed axes in a common plane. The schematic view in panels A–E is introduced in Fig. 2(d). Panel A shows the trivial example from Fig. 2(a). Panel B shows the orthogonal axes example from Fig. 2(b). In panel C, the left axis is orthogonal, and the right axis is at an angle of 30° to the connecting line. In panel D, both axes are parallel and at an angle of approximately 54.74° to the connecting line. Panel E is again the trivial example rotated by 180° . At the bottom, the graph of one branch of relation (2) between the angles θ and ϕ (marked red in panels A–E) which set the rotation axes is shown [cf. Fig. 2(d)]. The positions of the different configurations are marked on the graph.

It should be noted that all input and output axes of the gears mentioned in the Introduction are parallel; moreover, most of them are, in fact, coaxial. We now consider two dipoles and seek inclined rotation axes lying in a common plane with the objective of creating a CGS. For an example showing that such states exist, see Figs. 2(b) and 2(d). In this example, the rotation axes are orthogonal. The obvious question is how many configurations exist for two dipoles

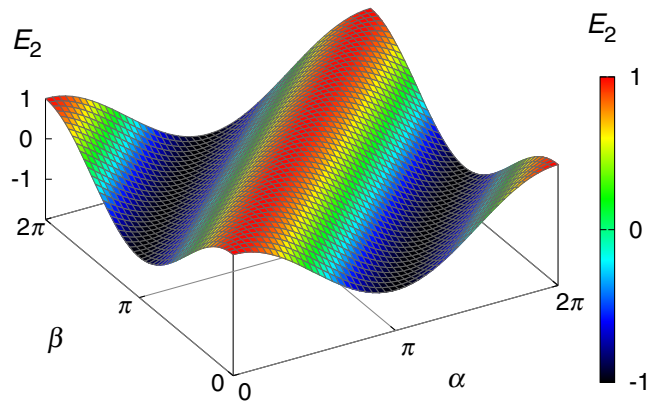


FIG. 4. Degenerate energy landscape (3) for two interacting dipoles ($m_1 = m_2 = d = 1$) obeying Eq. (2). The system is in its ground state if $\alpha - \beta = \pi$. Only in the trivial case of aligned rotation axes ($\theta = \varphi = 0$) this means the two dipoles are antiparallel in the ground state.

so that they form a CGS? It turns out that there are infinitely many. Referring to the definition of the angles θ and φ which fix the rotation axes of the two dipoles [cf. Figs. 1 and 2(d)], for every choice of θ there exists a φ which creates a CGS. The condition can be expressed as the nonlinear relation (see Appendix A)

$$\cos \theta \cos \varphi - 2 \sin \theta \sin \varphi = 1. \quad (2)$$

In view of Eq. (2), every angle between the two rotation axes can be realized. In Fig. 3, we show some notable configurations in the schematic view introduced in Fig. 2(d) together with the graph of one branch of the relation between θ and φ implied by Eq. (2). The second branch (obtained by reflecting the depicted branch over the line $\theta = \varphi$) does not contain new configurations up to symmetries. The explicit formula for the depicted branch is given in Appendix D. For the continuum of possible rotation axes described by Eq. (2), the energy is independent of θ and φ and has the form (see Appendix A)

$$E_2 = \frac{m_1 m_2}{d^3} \cos(\alpha - \beta), \quad (3)$$

where m_1 and m_2 are the magnitudes of the moments, and d is the distance between the dipoles. Therefore, the dynamics of two rotating dipoles is identical for all configurations obeying Eq. (2) since the Hamiltonian has the same form. Figure 4 shows the energy landscape (3).

Note that if the restriction to specific rotation axes is dropped and free orientations in 3D space are allowed, so far, only one finite arrangement with a CGS is previously known: the case of eight dipoles at the corners of a cube [23]. Indeed, the discovery of the dipole cube provides the initial motivation for seeking other CGSs since it can be argued that this arrangement is a unique peculiarity. We

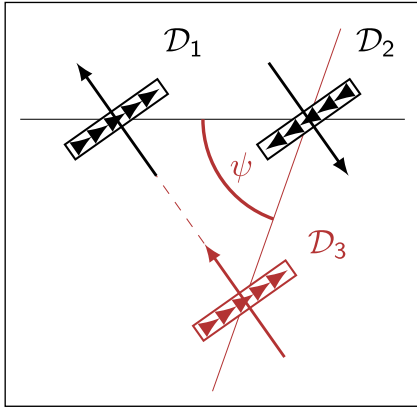
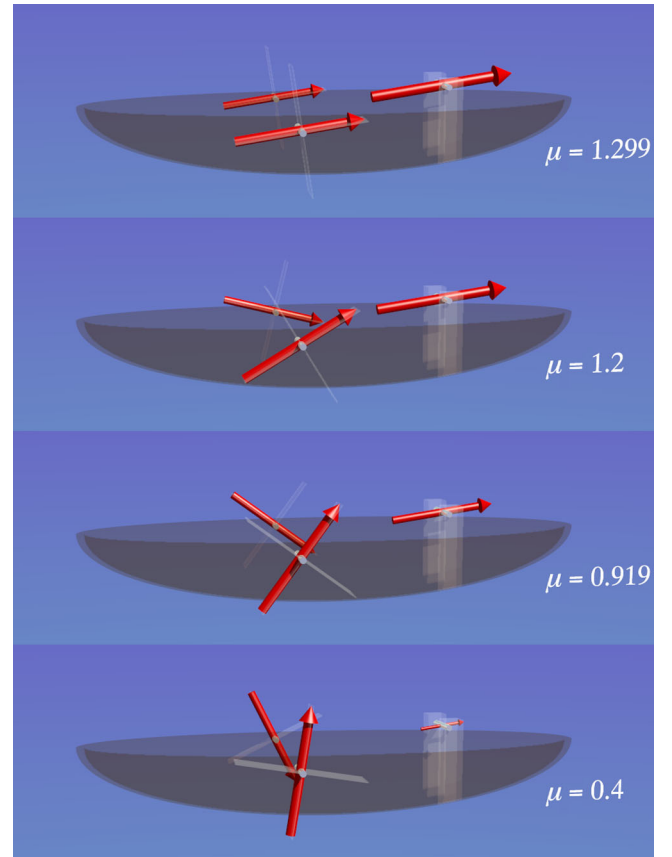


FIG. 5. Construction of a system with three interacting dipoles which form a continuous state. This construction begins with the configuration shown in Fig. 3, panel *D* and then the dipole \mathcal{D}_3 is added. The dipole pair $\mathcal{D}_2\mathcal{D}_3$ interacts in the same way as $\mathcal{D}_1\mathcal{D}_2$, while $\mathcal{D}_1\mathcal{D}_3$ forms the trivial continuum with aligned axes. The angle $\psi = 2 \arcsin(1/\sqrt{3}) \approx 70.53^\circ$ and the distances $\overline{\mathcal{D}_1\mathcal{D}_2}$ and $\overline{\mathcal{D}_2\mathcal{D}_3}$ are equal. The paddle boat in Video 1 uses this construction.

stress that the restriction to specific rotation axes in the current paper constitutes a fundamentally different class of systems compared to the free orientations. The best example is the dipole-dipole case: put two dipoles next to each other and let them orient freely in 3D space, they will align their moments coaxial head to tail and form a discrete (noncontinuous) ground state. For free orientations, not any one of the proposed mechanisms in this paper will work. For engineering applications, the restriction to rotation axes has an even greater practical significance because the primary concern is with the transmission of torques from one axis to one or several other axes. But the dipole cube [23] is also a solution for this class of problems if we choose the rotation axes as the respective volume diagonals of the cube: because even if the dipoles can be freely oriented in the cube, they actually force each other into planes orthogonal to the respective volume diagonal.

III. THREE INTERACTING DIPOLES

We next use the results for two dipoles to construct a system of three interacting dipoles which form a CGS and, therefore, act as gears which transmit mechanical torques. For this three dipole system to be a continuous state, every pair of dipoles needs to form such a state. For the configuration shown in Fig. 3, panel *D*, it is possible to add another dipole at the position shown in Fig. 5, while keeping the continuous state. The additional dipole \mathcal{D}_3 interacts with \mathcal{D}_2 exactly in the same way as the pair $\mathcal{D}_1\mathcal{D}_2$ does, whereas the pair $\mathcal{D}_1\mathcal{D}_3$ forms the trivial continuum with aligned axes. The configuration in Fig. 5 conveys the notion underlying the construction of the paddle boat in Video 1. From symmetry arguments, one might assume that for the system to work, the dipoles \mathcal{D}_1 and \mathcal{D}_3 need to be



VIDEO 2. (Animated version online.) The behavior for the system of three dipoles using the paddle boat construction from Video 1 as an example. The ratio of the driver dipole moment magnitude to the paddle dipole moment magnitude is at the critical value μ_c (top panel) or below μ_c (lower panels). The size of the driver dipole (right) is proportional to its dipole moment magnitude. The inclination angle between the paddle dipoles (left) is constant during rotation.

oriented parallel (like in Video 1). This configuration corresponds to the maximum energy state for the pair $\mathcal{D}_1\mathcal{D}_3$, which is unstable. That raises the question how the overall system can be in its stable ground state. The idea is to increase m_2 to make this particular configuration stable (with m_i we denote the magnitude of the dipole moment \mathbf{m}_i of \mathcal{D}_i). For the stability analysis of the possible equilibria, we assume $m_1 = m_3$ and define the magnitude ration $\mu := m_2/m_1$. For a critical ratio

$$\mu_c = \frac{3\sqrt{3}}{4} \approx 1.299, \quad (4)$$

the system undergoes a pitchfork bifurcation. If $\mu \geq \mu_c$, the dipoles \mathcal{D}_1 and \mathcal{D}_3 are parallel. Interesting enough, for $\mu < \mu_c$ the two stable states are both CGS (an “additional” twofold degeneracy). In these states, the dipoles \mathcal{D}_1 and \mathcal{D}_3 are inclined with respect to their common axis and maintain this inclination during the rotation in the continuous state analogous to a rigid body rotation; see Video 2. Denoting

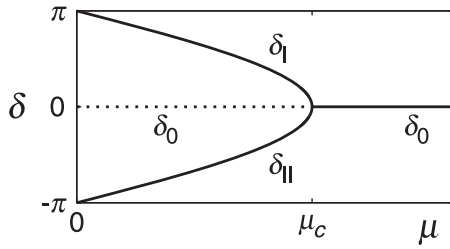


FIG. 6. Bifurcation diagram for the system of three dipoles showing the stable (solid lines) and unstable (dotted line) inclination angles δ between dipole \mathcal{D}_1 and \mathcal{D}_3 as a function of the dipole moment ratio $\mu := m_2/m_1$; see Eq. (5). At μ_c , a pitchfork bifurcation occurs.

the inclination angle with δ , we can characterize the three states which are stable for at least some values of μ as (see Appendix B)

$$\delta_0 = 0, \quad \delta_{i,||} = \pm 2 \arccos \frac{\mu}{\mu_c} \quad (5)$$

and show them in Fig. 6. With the decrease of μ , the angles $\delta_{i,||}$ grow in magnitude until \mathcal{D}_1 and \mathcal{D}_3 reach their trivial antiparallel ground state when μ is zero (i.e., \mathcal{D}_2 vanishes). From the Hessian matrix for the energy of the system, we obtain the eigenvalues (EVs) for the three states

$$\text{EV}_0 = \begin{bmatrix} 0 \\ 6s \\ 2(s-1) \end{bmatrix}, \quad \text{EV}_{i,||} = \begin{bmatrix} 0 \\ 6s^2 \\ 2(1-s^2) \end{bmatrix}, \quad (6)$$

with $s := \mu/\mu_c$. The first zero EV in all three states reflects again the degeneracy of any state of the system, and the corresponding eigenvector is $(1, 1, 1)^T$ in the space spanned by the angles α, β, γ which describe the actual orientations of the three dipoles. The second EV in all three states has the eigenvector $(-1, 2, -1)^T$ describing the joint rotation of \mathcal{D}_1 and \mathcal{D}_3 against the “natural” rotation. The system is always stable against perturbations in this direction since the EV is always positive (for $\mu > 0$). The third EV in all three states has the eigenvector $(-1, 0, 1)^T$ and describes the relative rotation between \mathcal{D}_1 and \mathcal{D}_3 . For $\mu > \mu_c$, perturbations in this direction are stable for δ_0 . At $\mu = \mu_c$, the pitchfork bifurcation occurs, so that for $\mu < \mu_c$, perturbations in this direction are unstable for δ_0 and stable for $\delta_{i,||}$; see Fig. 6. An animation of the system for different values of μ is given in Video 2.

IV. THE QUADRUPOLE-DIPOLE SYSTEM

An interesting generalization of the findings for two dipoles acting as gears involves higher multipole moments and combinations thereof. We consider the interaction

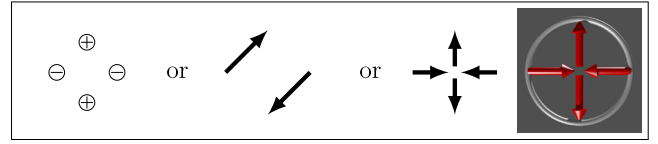


FIG. 7. Different ways to construct a point quadrupole. Left: Four monopoles of strength $\pm\sigma$ describing a square of area A are brought together ($A \rightarrow 0$) while σ is increased such that the product σA stays finite. Middle: Two antiparallel dipoles are brought together. Right: Four dipoles are brought together; this arrangement is used as a schematic visualization in Video 3.

between a quadrupole and a dipole, where the geometry is assumed as before: the rotation axes of the two objects lie in a common plane; the orientation of the quadrupole with respect to its rotation axis is analogous to the dipole in the sense that if one considers the quadrupole made up of four monopoles, these monopoles lie in the plane orthogonal to the rotation axis (Fig. 7). The interaction energy between a quadrupole at the origin and a dipole at position \mathbf{r} reads (see Appendix C)

$$E_{\text{QD}} = \frac{2|\mathbf{r}|^2(\mathbf{m}^T \mathbf{Q} \mathbf{r}) - 5(\mathbf{m} \cdot \mathbf{r})(\mathbf{r}^T \mathbf{Q} \mathbf{r})}{2|\mathbf{r}|^7}, \quad (7)$$

where \mathbf{Q} is the quadrupole moment tensor, and \mathbf{m} is the dipole moment. If we introduce the coordinate system analogous to Fig. 1, we again find a φ for every θ which creates a CGS. The respective nonlinear condition is (see Appendix C)

$$2 \cos \theta \cos \varphi - 3 \sin \theta \sin \varphi = 2. \quad (8)$$

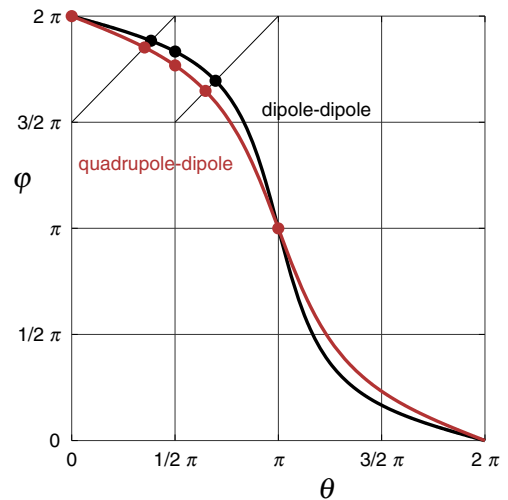
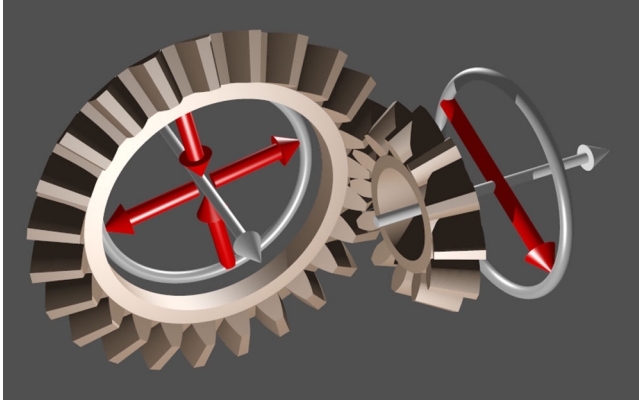


FIG. 8. The graph of one branch of relation (8) is shown in red, where the angles θ and ϕ define the rotation axes of the quadrupole-dipole system (see Figs. 2 and 3 for further explanations). As a comparison, the relation (2) for the dipole-dipole case is shown in black. The configurations from Fig. 3 are marked with filled circles.



VIDEO 3. (Animated version online.) Example of a continuous ground state created by a quadrupole and a dipole (shown in red) which are allowed to rotate about two orthogonal axes (shown in gray). The quadrupole (left) is symbolized by four dipoles. The mechanical bevel gears are added to illustrate an analogy to a mechanical system with a gear ratio of 1:2.

In contrast to the dipole-dipole case, the quadrupole-dipole system yields a gear ratio of 1:2. If a dipole is thought of as a gear with one “tooth” at the north pole and one “notch” at the south pole, a quadrupole is a gear with two teeth and two notches. When the dipole is rotated by a full cycle, the quadrupole rotates only half a cycle. An example of the quadrupole-dipole system is depicted in Video 3, whereas the graph of one branch of relation (8) is shown in Fig. 8. The explicit form of the interaction energy for the configurations obeying Eq. (8) reads (see Appendix C)

$$E_{\text{QD}} = -\frac{qm}{d^4} \sin \theta \cos(2\alpha - \beta), \quad (9)$$

where q and m are the magnitudes of the quadrupole and dipole moment, respectively, and d is the distance between the two objects. The energy landscape (9) is depicted in Fig. 9. The form of the energy (9) reflects the interesting effect that a quadrupole and a dipole do not “see” each other if the dipole is positioned anywhere along the rotation axis of the quadrupole, because this case corresponds to $\theta = 0, \pi$ for which $E_{\text{QD}} = 0$. There is no such phenomenon in the dipole-dipole case, where E_2 does not depend on θ or φ . As with the dipole systems discussed before, it is now possible to construct systems with more than one dipole or quadrupole. Again, for these systems to be in a continuous state, each pair of multipoles has to form such a state. The possibilities are even more diverse now since we can construct systems where certain quadrupole-dipole pairs do not see each other (cf. above). Generally, it is an intriguing puzzle to find a CGS for an increasing number of multipoles. A systematic strategy for doing so has not yet been proposed. One of many possible extensions is the inclusion of static (nonrotating) multipoles.

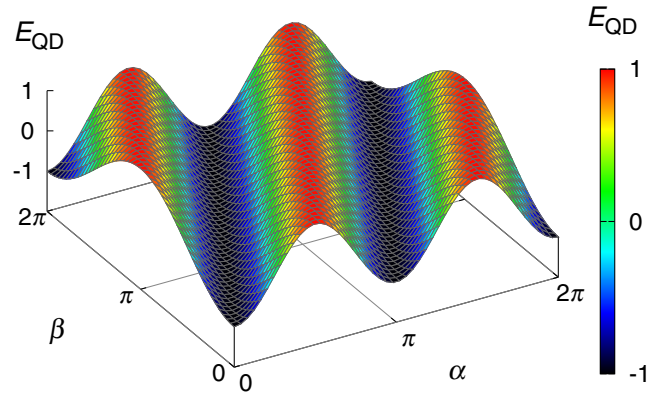


FIG. 9. Degenerate energy landscape (9) for the interaction of a quadrupole and a dipoles ($q = m = d = 1$, $\theta = \pi/2$) giving rise to a continuous ground state for $2\alpha = \beta$.

V. CONCLUDING REMARKS

Although the main purpose of this paper is the introduction of a gear concept based on a symmetry for multipole interactions, we comment on some technical aspects regarding the actual realization of the corresponding machines. The analysis relies on the assumption of ideal point multipoles. For the case of dipole systems, we can make use of the fact that a homogeneously magnetized sphere creates an outer field identical to a point dipole at the center of the sphere. Whether there exists an analogue principle for higher-order moments is an interesting question by itself: is there a shape with a specific magnetization pattern which creates an outer field identical to a point quadrupole?

Regarding characteristics such as torque densities, the theoretical analysis for a concrete application is straightforward since the expressions for the interaction energies are readily given in analytical form. The characteristics should qualitatively resemble those in Refs. [21,22].

Concerning the direct applicability in an actual machine, it is noted that we are already working on an experimental realization of a car drive based on the three-dipole system in Fig. 5, which is also the basis of the design in Video 1. The system is realized with inch-sized neodymium magnetic spheres and 3D printer technology. Engineering characteristics, like, for example, the transmittable torque densities, off-axis torques (which will bend the axes), or frictional losses at the bearings, can be investigated once the prototype for the drive is finished. The results will be reported in a forthcoming publication.

As indicated in the Introduction, other potential applications can be found in the area of microfluidic systems, where especially the possibility of transmitting torques into a physically isolated domain is an advantage of magnetic mechanisms over mechanical ones. On the length scales of nanotechnology, we can even think about the construction of the proposed mechanisms with electric multipoles. All

the findings in this paper are, of course, valid for magnetic as well as electric systems.

ACKNOWLEDGMENTS

The author is very grateful to Eliot Fried and Ingo Rehberg for many inspiring discussions and kind support.

APPENDIX A: THE ENERGY FOR TWO DIPOLES

From Fig. 1, we infer the components of the two-dipole moment vectors to be

$$\mathbf{m}_1 = m_1 \begin{pmatrix} -\cos \alpha \sin \theta \\ \cos \alpha \cos \theta \\ \sin \alpha \end{pmatrix}, \quad (\text{A1})$$

$$\mathbf{m}_2 = m_2 \begin{pmatrix} -\cos \beta \sin \varphi \\ \cos \beta \cos \varphi \\ \sin \beta \end{pmatrix}, \quad (\text{A2})$$

with m_1 and m_2 being the magnitudes of the moments. We assume the distance between the dipoles to be d and their positions to be $(0, 0, 0)^T$ and $(d, 0, 0)^T$, respectively. Now we can introduce Eqs. (A1) and (A2) into Eq. (1) and get

$$E_2 = \frac{m_1 m_2}{d^3} [\cos \alpha \cos \beta (\cos \theta \cos \varphi - 2 \sin \theta \sin \varphi) + \sin \alpha \sin \beta]. \quad (\text{A3})$$

If we treat θ and φ as fixed parameters, then E_2 is a function $E_2(\alpha, \beta)$. The only way to create a degeneracy in the energy landscape $E_2(\alpha, \beta)$ is to set the term in round brackets in Eq. (A3) to unity, i.e.,

$$\cos \theta \cos \varphi - 2 \sin \theta \sin \varphi = 1, \quad (\text{A4})$$

which is exactly the condition (2). Because only if Eq. (A4) holds, Eq. (A3) can be written as

$$E_2 = \frac{m_1 m_2}{d^3} [\cos \alpha \cos \beta + \sin \alpha \sin \beta] \quad (\text{A5})$$

$$= \frac{m_1 m_2}{d^3} \cos(\alpha - \beta). \quad (\text{A6})$$

Because of the degeneracy, the Hessian of E_2 has a zero eigenvalue in the entire space spanned by α and β , the corresponding eigenvector being $(1, 1)^T$.

APPENDIX B: STABILITY ANALYSIS FOR THE SYSTEM OF THREE DIPOLES

Referring to Fig. 5, we denote the distance between dipole \mathcal{D}_i and \mathcal{D}_j with d_{ij} , the magnitudes of the dipole moments with $m_{1,2,3}$, and the angles describing the actual

orientation of the dipoles with α, β, γ . Further, we assume $m_1 = m_3$ and define the dipole moment ratio $\mu := m_2/m_1$. Without loss of generality, we can set $m_{1,3} = d_{13} = 1$. It then follows from geometry that $d_{12} = d_{23} = \sqrt{3}/2$. Since all three pairwise interactions of the system form a degenerate continuous state, we can use Eq. (A6) to write down the energy E_3 of this system as

$$E_3 = k[\cos(\alpha - \beta) + \cos(\beta - \gamma)] + \cos(\alpha - \gamma), \quad (\text{B1})$$

with $k := 8\mu/(3\sqrt{3})$. The respective gradient reads

$$\text{grad}E_3 = \begin{pmatrix} -\sin(\alpha - \gamma) - k \sin(\alpha - \beta) \\ \sin(\alpha - \gamma) - k \sin(\gamma - \beta) \\ k \sin(\alpha - \beta) + k \sin(\gamma - \beta) \end{pmatrix}. \quad (\text{B2})$$

There are four families of degenerate equilibria (states with $\text{grad}E_3 = 0$). We discuss only the two families which are stable for at least some values of μ . They are covered by the ansatz

$$\alpha = \beta + \pi + \delta/2, \quad \gamma = \beta + \pi - \delta/2. \quad (\text{B3})$$

The angle δ describes the inclination of \mathcal{D}_1 and \mathcal{D}_3 with respect to their common axis as discussed in the main text. Introducing Eq. (B3) into Eq. (B2) and equating to zero, we find that the third component of Eq. (B2) is always zero, and the first and second component result in the same condition

$$\sin \frac{\delta}{2} \left(2 \cos \frac{\delta}{2} - k \right) = 0. \quad (\text{B4})$$

The three relevant solutions to Eq. (B4) are the states

$$\delta_0 = 0, \quad \delta_{i,\parallel} = \pm 2 \arccos \frac{k}{2}. \quad (\text{B5})$$

The fourth solution $\delta = \pi$ is always unstable and not considered here. For the state δ_0 , the dipoles \mathcal{D}_1 and \mathcal{D}_3 are parallel, whereas for the states $\delta_{i,\parallel}$ they are inclined. The solutions $\delta_{i,\parallel}$ do exist only below the critical value of $\mu_c = 3\sqrt{3}/4$. For the stability analysis, we compute the eigenvalues and vectors of the Hessian matrix of E_3 for the three states δ_0 and $\delta_{i,\parallel}$ using Eqs. (B3) and (B5). The result is given in the main text.

APPENDIX C: THE ENERGY FOR THE QUADRUPOLE-DIPOLE CASE

There are several ways to construct a point quadrupole from a limit process for the positioning of point dipoles or monopoles. Figure 7 illustrates some constructions. For the derivation of the quadrupole moment tensor, we use the monopole construction (Fig. 7 left), and the coordinate

system as introduced in Fig. 1. We assume the upper monopole position in Fig. 7 left to be described with the left dipole moment vector in Fig. 1 and the other three monopoles to lie in the plane orthogonal to the rotation axis. Then we can write down the monopole positions (counting from the upper monopole in the clockwise direction 1, 2, 3, 4)

$$\mathbf{p}_1 = \epsilon \begin{pmatrix} -\cos \alpha \sin \theta \\ \cos \alpha \cos \theta \\ \sin \alpha \end{pmatrix}, \quad \mathbf{p}_2 = \epsilon \begin{pmatrix} -\sin \alpha \sin \theta \\ \sin \alpha \cos \theta \\ -\cos \alpha \end{pmatrix}, \quad (\text{C1})$$

$\mathbf{p}_3 = -\mathbf{p}_1$ and $\mathbf{p}_4 = -\mathbf{p}_2$. The factor ϵ contains the length scale. The symmetric traceless quadrupole moment tensor is commonly defined as

$$Q_{ij} = \sum_k c_k (3p_{ki}p_{kj} - \delta_{ij}|\mathbf{p}_k|^2), \quad (\text{C2})$$

where p_{ki} is the component i of \mathbf{p}_k , c_k is the monopole's strength, and δ_{ij} is the Kronecker delta. Now we introduce the positions (C1) together with $c_{1,3} = \sigma$ and $c_{2,4} = -\sigma$ into Eq. (C2) and consider the limit $\sigma\epsilon^2 \rightarrow q/6$ (cf. Fig. 7). q describes the magnitude of the quadrupole moment, and without loss of generality, the factor $1/6$ is added to reduce the numerical prefactors in the final result. We then arrive at the quadrupole tensor components

$$\begin{aligned} Q_{xx} &= -a \sin^2 \theta, \\ Q_{yy} &= -a \cos^2 \theta, \\ Q_{zz} &= a, \\ Q_{xy} &= a \sin \theta \cos \theta, \\ Q_{xz} &= -Q_{yz} = -2q \sin \alpha \cos \alpha \cos \theta, \end{aligned} \quad (\text{C3})$$

where $a := q(\sin^2 \alpha - \cos^2 \alpha)$. Now the potential at a spatial position \mathbf{r} due to the quadrupole at the origin can be expressed as

$$\phi = \frac{1}{2} \frac{\mathbf{r}^T \mathbf{Q} \mathbf{r}}{|\mathbf{r}|^5}. \quad (\text{C4})$$

With the corresponding force field of the quadrupole $\mathbf{F} = -\text{grad}\phi$, we can write the interaction energy between the quadrupole at the origin and a dipole with dipole moment \mathbf{m} at position \mathbf{r} as $E_{\text{QD}} = -\mathbf{m} \cdot \mathbf{F} = \mathbf{m} \cdot \text{grad}\phi$ resulting in

$$E_{\text{QD}} = \frac{2|\mathbf{r}|^2(\mathbf{m}^T \mathbf{Q} \mathbf{r}) - 5(\mathbf{m} \cdot \mathbf{r})(\mathbf{r}^T \mathbf{Q} \mathbf{r})}{2|\mathbf{r}|^7}. \quad (\text{C5})$$

Introducing Eq. (C3) and

$$\mathbf{m} = m \begin{pmatrix} -\cos \beta \sin \varphi \\ \cos \beta \cos \varphi \\ \sin \beta \end{pmatrix} \quad (\text{C6})$$

together with $\mathbf{r} = (d, 0, 0)^T$ into Eq. (C5), we finally obtain

$$E_{\text{QD}} = -\frac{qm}{d^4} \sin \theta [G \cos(2\alpha) \cos \beta - \sin(2\alpha) \sin \beta],$$

$$\text{where } G := \cos \theta \cos \varphi - \frac{3}{2} \sin \theta \sin \varphi. \quad (\text{C7})$$

Again, like in the dipole-dipole case, the only way to create a degeneracy in the energy landscape $E_{\text{QD}}(\alpha, \beta)$ is to set $G = 1$, i.e.,

$$2 \cos \theta \cos \varphi - 3 \sin \theta \sin \varphi = 2, \quad (\text{C8})$$

which is exactly the condition for degeneracy in the main text. Because only if Eq. (C8) holds, the energy can be written as

$$E_{\text{QD}} = -\frac{qm}{d^4} \sin \theta \cos(2\alpha - \beta). \quad (\text{C9})$$

APPENDIX D: EXPLICIT FORMULAS FOR THE RELATIONS BETWEEN θ AND φ

The relation between θ and φ for the dipole-dipole case

$$\cos \theta \cos \varphi - 2 \sin \theta \sin \varphi = 1 \quad (\text{D1})$$

has the explicit form

$$\varphi = \text{atan2}[\sin \theta(\sqrt{3} \cos \theta - 2), 2\sqrt{3} \sin^2 \theta + \cos \theta] \quad (\text{D2})$$

for the branch shown in Fig. 3 of the main text. For the definition of the function atan2 , see [24]. The relation between θ and φ for the quadrupole-dipole case

$$2 \cos \theta \cos \varphi - 3 \sin \theta \sin \varphi = 2 \quad (\text{D3})$$

has the explicit form

$$\varphi = \text{atan2}[2 \sin \theta(\sqrt{5} \cos \theta - 3), 3\sqrt{5} \sin^2 \theta + 4 \cos \theta] \quad (\text{D4})$$

for the branch shown in Fig. 8 of the main text.

-
- [1] Ala'aldeen Al-Halhouli, Stefanie Demming, Andreas Waldschik, and Stephanus Büttgenbach, Implementation of synchronous micromotor in developing integrated microfluidic systems, *Micromachines* 5, 442 (2014).
 - [2] Wesley T. E. van den Beld, Natalia L. Cadena, Johan Bomer, Eddy L. de Weerd, Leon Abelmann, Albert van den Berg,

- and Jan C. T. Eijkel, Bidirectional microfluidic pumping using an array of magnetic Janus microspheres rotating around magnetic disks, *Lab Chip* **15**, 2872 (2015).
- [3] Mark Peplow, The tiniest Lego: A tale of nanoscale motors, rotors, switches and pumps, *Nature (London)* **525**, 18 (2015).
- [4] P. M. Tlali, R.-J. Wang, and S. Gerber, Magnetic gear technologies: A review, in *Proceedings of International Conference on Electrical Machines (ICEM), 2014* (IEEE, Berlin, 2014), pp. 544–550.
- [5] C. G. Armstrong, Power-transmitting device, U.S. Patent No. 687,292 (Nov. 26, 1901).
- [6] K. Tsurumoto and S. Kikuchi, A new magnetic gear using permanent magnet, *IEEE Trans. Magn.* **23**, 3622 (1987).
- [7] K. Atallah and D. Howe, A novel high-performance magnetic gear, *IEEE Trans. Magn.* **37**, 2844 (2001).
- [8] Kais Atallah, Stuart D. Calverley, and David Howe, High-performance magnetic gears, *J. Magn. Magn. Mater.* **272–276**, E1727 (2004).
- [9] S. Mezani, K. Atallah, and D. Howe, A high-performance axial-field magnetic gear, *J. Appl. Phys.* **99**, 08R303 (2006).
- [10] K. T. Chau, Dong Zhang, J. Z. Jiang, and Linni Jian, Transient analysis of coaxial magnetic gears using finite element comodeling, *J. Appl. Phys.* **103**, 07F101 (2008).
- [11] A. Ya. Krasilnikov and A. A. Krasilnikov, Torque determination for a cylindrical magnetic clutch, *Russ. Eng. Res.* **29**, 544 (2009).
- [12] Xinhua Liu, K. T. Chau, J. Z. Jiang, and Chuang Yu, Design and analysis of interior-magnet outer-rotor concentric magnetic gears, *J. Appl. Phys.* **105**, 07F101 (2009).
- [13] Linni Jian, K. T. Chau, Yu Gong, J. Z. Jiang, Chuang Yu, and Wenlong Li, Comparison of coaxial magnetic gears with different topologies, *IEEE Trans. Magn.* **45**, 4526 (2009).
- [14] Linni Jian and K. T. Chau, A coaxial magnetic gear with Halbach permanent-magnet arrays, *IEEE Trans. Energy Convers.* **25**, 319 (2010).
- [15] Kenji Nakamura, Michinari Fukuoka, and Osamu Ichinokura, Performance improvement of magnetic gear and efficiency comparison with conventional mechanical gear, *J. Appl. Phys.* **115**, 044301 (2014).
- [16] Ping Zheng, Jingang Bai, Jia Lin, Zhenxing Fu, Zhiyi Song, and Fei Lin, Design and transient behavior of magnetic gears, *J. Appl. Phys.* **115**, 17E706 (2014).
- [17] Cheng-Chi Huang, Mi-Ching Tsai, D. G. Dorrell, and Bor-Jeng Lin, Development of a magnetic planetary gearbox, *IEEE Trans. Magn.* **44**, 403 (2008).
- [18] F. T. Jorgensen, T. O. Andersen, and P. O. Rasmussen, The cycloid permanent magnetic gear, *IEEE Trans. Ind. Appl.* **44**, 1659 (2008).
- [19] J. F. Charpentier and G. Lemarquand, Mechanical behavior of axially magnetized permanent-magnet gears, *IEEE Trans. Magn.* **37**, 1110 (2001).
- [20] F. T. Jorgensen, T. O. Andersen, and P. O. Rasmussen, Two dimensional model of a permanent magnet spur gear, in *Proceedings of the Industry Applications Conference, 2005* (IEEE, New York, 2005), Vol. 1, pp. 261–265.
- [21] E. P. Furlani, Formulas for the force and torque of axial couplings, *IEEE Trans. Magn.* **29**, 2295 (1993).
- [22] E. P. Furlani, Analysis and optimization of synchronous magnetic couplings, *J. Appl. Phys.* **79**, 4692 (1996).
- [23] Johannes Schönke, Tobias M. Schneider, and Ingo Rehberg, Infinite geometric frustration in a cubic dipole cluster, *Phys. Rev. B* **91**, 020410 (2015).
- [24] <https://en.wikipedia.org/wiki/Atan2>.